Application of curvatures to airborne gravity gradients

Carlos Cevallos
Fugro Airborne Surveys
Perth, Western Australia
ccevallos@
fugroairbone.com.au

Mark Dransfield
Fugro Airborne Surveys
Perth, Western Australia
mdransfield@
fugroairbone.com.au

Jacqueline Hope
Fugro Airborne Surveys
Perth, Western Australia
jhope@
fugroairbone.com.au

Heather Carey
Fugro Airborne Surveys
Perth, Western Australia
hcarey@
fugroairbone.com.au

SUMMARY

The application of equipotential surface curvatures to airborne gravity gradient data is presented. The differential curvature, as measured by the FALCON™ airborne gravity gradiometer system, the mean curvature, and the direction of maximum curvature of the equipotential surface should improve the understanding and geological interpretation of gravity gradient data.

It has been shown that the horizontal gradients of the vertical component of the gravity vector form the curvature of the gravity field line. As this line is orthogonal to the equipotential surface, its curvature is related to how successive equipotential surfaces change and it may not be needed to interpret.

The theoretical basis for the method is discussed. Practical applications of utilising the curvature method are presented on a synthetic model and FALCON™ airborne gravity gradiometer data from the western zone of the Halls Creek Orogen, Western Australia.

Keywords: Gravity, gradients, equipotential, curvature, FALCON™

INTRODUCTION

After twelve years of application in exploration geophysics (van Leeuwen, 2000; Lee, 2001), airborne gravity gradiometry is now an established technique that provides very accurate measurements of the spatial variations in the gravity field from an aircraft.

The common approach of expressing the gravity gradient tensor field in terms of its Cartesian representation provides nine measured values (five of them locally independent) at each point and these values are each dependent on the choice of coordinates. This complexity has led to interpreters either simplifying their task by only using the vertical gravitational acceleration and its first vertical derivative or exploiting the mathematical properties of the tensor to examine its invariant properties (Pedersen and Rasmussen, 1990).

We prefer to use the physical properties of the gravity gradient tensor in order to understand what it is telling us about the variations in the earth's field and therefore in the geology. As we shall show, the gravity gradient tensor has a physical and geometrical meaning which is independent of any coordinate representation and is not simply a mathematical construct. The gravity gradient is the curvature of the potential.

Close to massive bodies we expect the potential field to be strongly curved and when those bodies are elongated in any direction, we expect the curvature to be greatest perpendicular to that direction. Thus there should be a clear physical relationship between the gradient and the geology expressed in terms of the curvature.

In this paper, we seek to determine what gravity gradient information is sufficient and necessary to interpret both structural and lithological features, and to estimate the density distribution in the subsurface environment. We begin with a brief introduction of the gravity gradient tensor. Although our ideas are physical, we need to express this mathematically and so we review curvature theory and show the main results.

We demonstrate the practical applications of utilising the curvature method on a synthetic model and FALCON™ AGG data from the western zone of the Halls Creek Orogen, Western Australia.

THEORY

The gravity gradient tensor

The gravity field, **g**, in domains outside density distributions satisfies:

$$\nabla \times \mathbf{g} = 0 \tag{1}$$
$$\nabla \bullet \mathbf{g} = 0 \tag{2}$$

Instead of solving two vector field equations for **g**, an equivalent solution to a more complex but scalar equation can be sought if the gravity field is expressed by the gravity potential, φ:

$$\mathbf{g} = \nabla \boldsymbol{\varphi} \tag{3}$$
$$\nabla \times \nabla \boldsymbol{\varphi} = 0 \tag{4}$$
$$\nabla \bullet \nabla \boldsymbol{\varphi} = \nabla^2 \varphi = 0 \tag{5}$$

where equation (3) satisfies equation (1), and equation (4) transforms vector equation (2) into the scalar equation (5).

We are interested in spatial variation in the gravity field, that is, spatial derivatives of components of the gravity vector field, which are the second spatial derivatives of the gravity potential. The potential is a scalar (or rank zero tensor) field, the gravity is a vector (rank one tensor) field and the second spatial derivatives of the potential form a rank two tensor field, commonly called the gravity gradient tensor.

In the three orthogonal directions x, y, and z, **g** is represented by a three dimensional vector (g_x, g_y, g_z) and the gravity gradient tensor by a matrix:

$$\begin{pmatrix} \varphi_{xx} & \varphi_{xy} & \varphi_{xz} \\ \varphi_{yx} & \varphi_{yy} & \varphi_{yz} \\ \varphi_{zx} & \varphi_{zy} & \varphi_{zz} \end{pmatrix} \tag{6}$$

where the subscripts indicate partial differentiation with respect to the subscripted variable. A tensor is a physical field independent of the choice of coordinates and therefore distinct from its representation in those coordinates.

Curvatures

Expressions that relate curvature to potential can be found by defining a surface $z(x,y)$ and then relating it to an equipotential surface. The following theory follows the work of Slotnick (1932). The surface (Figure 1) is approximated to second order by an expansion of z in a Taylor series about the point of observation.

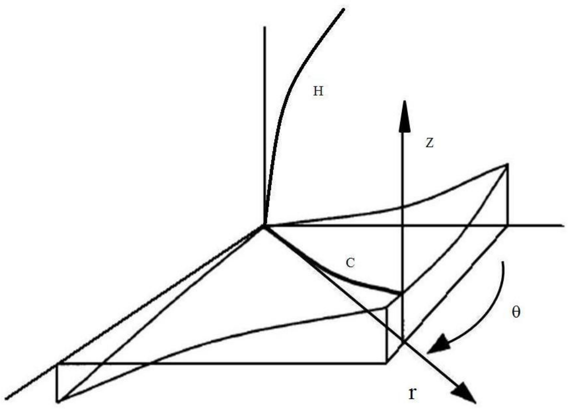

Figure 1. Surface modified from Slotnick. Curve C is tangent to r at origin and curve H is perpendicular to surface at origin.

Expanded in cylindrical coordinates, where r is a radius vector, z can be written in the form:

$$z = \frac{r^2}{2}\left(\frac{\partial^2 z}{\partial x^2}\cos^2\theta + 2\frac{\partial^2 z}{\partial xy}\cos\theta\sin\theta + \frac{\partial^2 z}{\partial y^2}\sin^2\theta\right) \tag{7}$$

Intersection of the surface with a vertical plane through the origin yields a curve; the curvature of the curve, κ, is given by applying the formula below to equation (7) which yields equation (9):

$$\frac{\frac{d^2 z}{dr^2}}{\left(1+\left(\frac{dz}{dr}\right)^2\right)^{3/2}} \tag{8}$$

$$\kappa = \frac{\partial^2 z}{\partial x^2}\cos^2\theta + 2\frac{\partial^2 z}{\partial xy}\cos\theta\sin\theta + \frac{\partial^2 z}{\partial y^2}\sin^2\theta \tag{9}$$

Calculating the maximum and minimum curvatures that occur at unique orthogonal angles and averaging them yields a constant termed the mean curvature (κ_m):

$$\kappa_m = \frac{1}{2}\left(\frac{\partial^2 z}{\partial x^2} + \frac{\partial^2 z}{\partial y^2}\right) \tag{10}$$

The difference between the maximum and minimum curvature is termed the differential curvature (κ_d), such that:

$$\kappa_d = \sqrt{\left(\frac{\partial^2 z}{\partial x^2} - \frac{\partial^2 z}{\partial y^2}\right)^2 + 4\left(\frac{\partial^2 z}{\partial xy}\right)^2} \tag{11}$$

Given that $\varphi(x, y, z)$ is constant, and $g = \varphi_z$, substitution into equation (10) yields:

$$\kappa_m = \frac{1}{2g}(\varphi_{xx} + \varphi_{yy}) \tag{12}$$

From equation (5) we note that:

$$\varphi_{xx} + \varphi_{yy} + \varphi_{zz} = 0 \tag{13}$$

By combining equations (12) and (13), we obtain the following results:

$$\kappa_m = -\frac{1}{2g}\varphi_{zz} \tag{14}$$

$$\kappa_d = \frac{1}{g}\sqrt{\varphi_\Delta^{\,2} + 4\varphi_{xy}^{\,2}}\ , \tag{15}$$

where

$$\varphi_\Delta = \varphi_{yy} - \varphi_{xx} \tag{16}$$

The curvature of surfaces and their application to gravity gradiometry are well known in differential geometry. Geophysicists using torsion balances in the 1930s were well acquainted with differential curvatures (Heiland, 1968). Another quantity traditionally measured by the torsion balance and commonly used in interpretation is the horizontal gradient of vertical gravity:

$$\sqrt{\varphi_{xz}^{\,2} + \varphi_{yz}^{\,2}} \tag{17}$$

This begs the question whether the quantity

$$\frac{1}{g}\sqrt{\varphi_{xz}^{\,2} + \varphi_{yz}^{\,2}} \tag{18}$$

reflects the curvature of something related to the equipotential surface. In fact, it is the curvature of the gravity field line. The following theory follows the geodesy work of Hofmann-Wellenhof and Moritz (2006). A gravity field line is a curve (curve H in Figure 1) whose line element vector ***ds*** is parallel to the gravity vector, **g**:

$$\boldsymbol{ds} = (dx, dy, dz) \tag{19}$$

$$\mathbf{g} = (\varphi_x, \varphi_y, \varphi_z) \tag{20}$$

That is, their components are proportional:

$$\frac{dx}{\varphi_x} = \frac{dy}{\varphi_y} = \frac{dz}{\varphi_z} \tag{21}$$

In Figure 1, the curvature of the projection of the gravity field line on the xy-plane is equal to κ_1, where:

$$\kappa_1 = \frac{\partial^2 x}{\partial z^2} \tag{22}$$

From (21), it follows that:

$$\frac{dx}{dz} = \frac{\varphi_x}{\varphi_z} \tag{23}$$

Differentiating with respect to z, as $y = 0$ yields:

$$\kappa_1 = \frac{1}{\varphi_z^{\,2}}\left[\varphi_z\left(\varphi_{xz} + \varphi_{xx}\frac{dx}{dz}\right) - \varphi_x\left(\varphi_{zz} + \varphi_{zx}\frac{dx}{dz}\right)\right] \tag{24}$$

The following sequential equations outline the theory used in our case to calculate the curvature of the gravity field line (κ_f):

$$\mathbf{g} = (0, 0, g) \quad (25)$$

$$\varphi_x = \varphi_y = 0 \quad (26)$$

$$\frac{dx}{dz} = 0 \quad (27)$$

$$\frac{\partial^2 x}{\partial z^2} = \frac{\varphi_z \varphi_{xz}}{\varphi_z^{\;2}} = \frac{\varphi_{xz}}{\varphi_z} = \frac{\varphi_{zx}}{\varphi_z} \quad (28)$$

$$\kappa_1 = \frac{1}{g}\varphi_{xz} \quad (29)$$

$$\kappa_2 = \frac{1}{g}\varphi_{yz} \quad (30)$$

$$\kappa_f = \sqrt{\kappa_1^{\;2} + \kappa_2^{\;2}} = \frac{1}{g}\sqrt{\varphi_{xz}^{\;2} + \varphi_{yz}^{\;2}} \quad (31)$$

The equipotential surface at a given point has six degrees of freedom: two curvatures, three angles, and the value of the surface. Restricting the *z* coordinate to be the "Down" coordinate (the direction perpendicular to the geoid), reduces the degrees of freedom of the angles to one. In theory, the interpretation of airborne gravity gradient data using only three quantities is possible; the mean curvature, differential curvature, and direction of the maximum (or minimum) curvature.

The gravity field line curvature does not add significant information about the equipotential surface. Gravity field lines and equipotential surfaces are considered equivalent since they are orthogonal (equation 3) and in regions devoid of mass they contain the same information.

MODELLING

The FALCON™ AGG system measures φ_Δ and φ_{xy}, and from these, φ_{zz} and g are derived. The resolution of the gravity gradient measurements can be as good as 3.0 eötvös and 0.15 milligals for gravity measurements. For FALCON™ data, the coordinate system is (North, East, Down) is $(N, E, D) = (x, y, z)$. The relevant quantities are: $\varphi_{DD} = \varphi_{zz}$, $\varphi_{UV} = \varphi_\Delta/2$, $\varphi_{NE} = \varphi_{xy}$ and $g_D = g$. Each point is on an equipotential surface for which we can obtain two curvatures, the mean curvature (κ_m) and the differential curvature (κ_d), and the strike direction of the maximum curvature (θ_κ):

$$\kappa_m = \frac{\varphi_{DD}}{2g_D} \quad (34)$$

$$\kappa_d = \frac{2}{g_D}\sqrt{\varphi_{UV}^{\;2} + \varphi_{NE}^{\;2}} \quad (35)$$

$$\theta_\kappa = \frac{1}{2}\operatorname{atan}\frac{\varphi_{NE}}{\varphi_{UV}} \quad (36)$$

In this section and the one following, our examples use the residual gravity gradient field after removal of the regional. The only significant consequence is in the range of values of the curvatures. At the surface, the earth's gravitational acceleration is about 9.8 ms^{-2} and its vertical gravity gradient about 3100 Eö, leading to a mean curvature of approximately 1.5 x 10^{-7} m^{-1}, consistent with its known radius of about 6,000 km. Our use of residual gradients gives values more than an order of magnitude smaller.

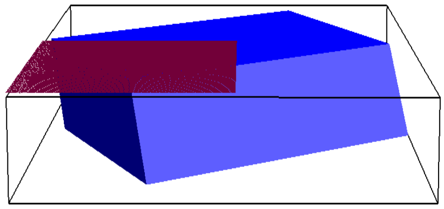

Figure 2. **Model 3D view looking south at a NNW-dipping block with a vertical NE edge.**

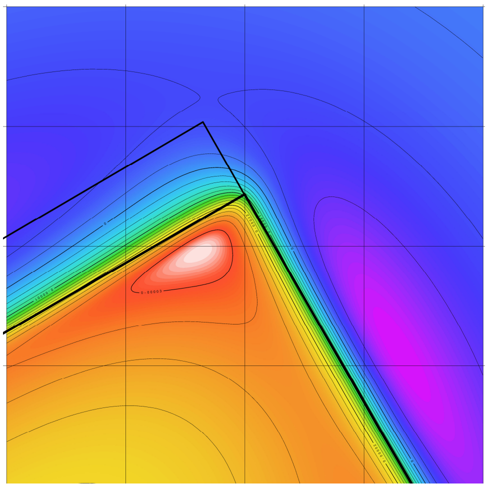

Figure 3. Mean curvature over the synthetic model. Values range from 3.1 x 10^{-5} m^{-1} (red) to 0.8 x 10^{-5} m^{-1} (purple).

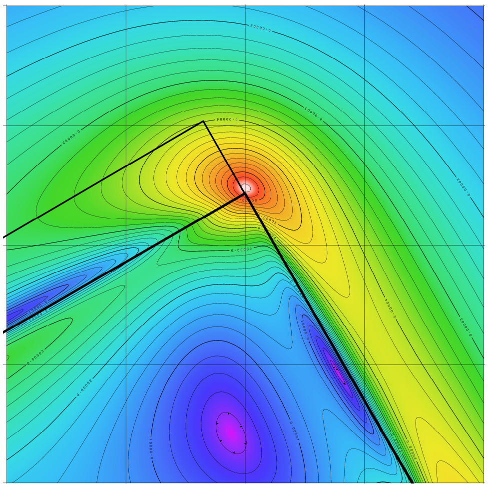

Figure 4. Differential curvature over the synthetic model. Values range from 6.4 x 10^{-5} m^{-1} (red) to 0.01 x 10^{-5} m^{-1} (purple).

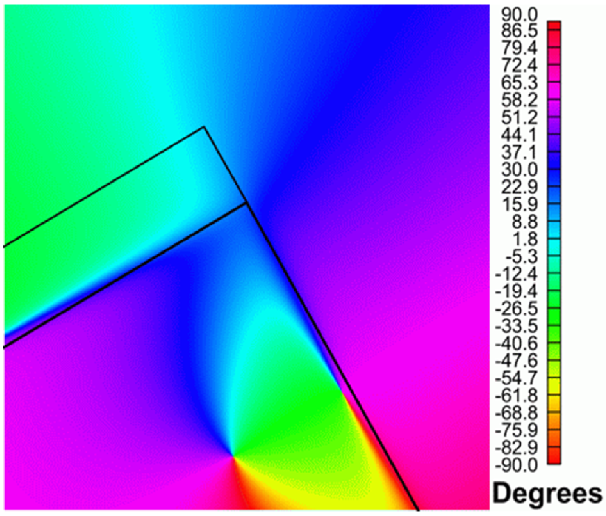

Figure 5. Strike of the maximum curvature over the synthetic model. Here, the north-south strikes of maximum curvature (strike angle of 0°) are shown in light blue, while east-west strike angles (either –90° or 90°) appear red.

The application of curvatures with existing interpretation methods was tested using a synthetic model (Figures 2, 3, 4 and 5). The model body was assigned a density contrast of 0.25 gm/cc, a 250 m depth-to-top of model, and 3 km body depth extent. The model body was also assigned a strike length of 15 km, 10 km width, and a 60^o dip towards the north-northwest. The curvature results of the model demonstrate how the mean curvature indicates the location of the mass distribution (Figures 3) whereas the differential curvature is clearly mapping the edges of the body (Figure 4). The strike of maximum curvature (Figure 5) maps the orientation of the nearest edge of the body, except near the corner. Thus the results are entirely consistent with our expectations.

APPLICATION

The curvature method was applied to FALCON™ AGG data from the western zone of the Halls Creek Orogen, Western Australia (Figure 6). The application of curvature information is presented here with the aim of simply illustrating how our understanding of the curvature relates to the geology.

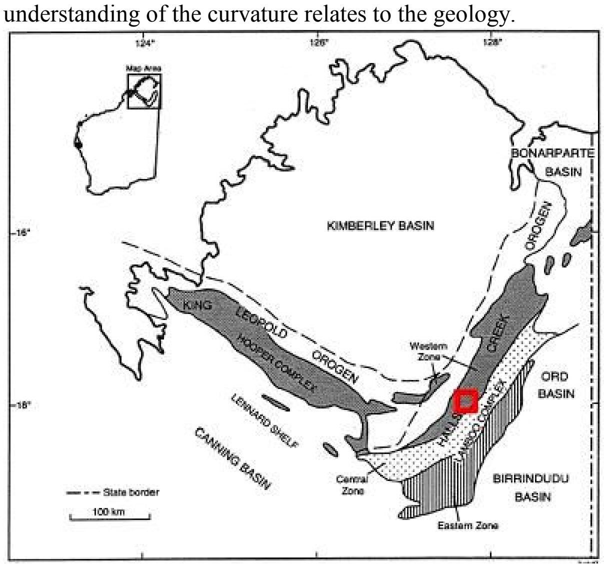

Figure 6. Sketch map outlining the Halls Creek Orogen in Western Australia (Sheppard et al., 1997). The AGG data area presented below are from the area outlined in red.

The geology over the area consists primarily of granitoids, dolerite, gabbro, and ultra-basic intrusions, and minor sedimentary units. The published 1:1M scale geology line work (modified from Stewart, A.J. et al., 2008) is overlain on Figures 7, 8 and 9 to display basic similarities and contrasts between the curvature data and this geology.

Generally, the mean curvature reflects the geographical distribution of dense sources. For illustrative purposes, we note three such dense features in Figure 7: feature A, a broad, generally featureless, circular high covering most of the north-west portion of the image; feature B, a north-south aligned linear feature with its northern end just below and to the east of the centre of the image; and feature C, a composite high (white coloured in the west, red in the east) that forms the dominant high signal in the south.

The differential curvature is a measure of the departure from symmetry of the density sources. We note that the differential curvature over features A and C is low indicating their symmetry although the break between the east and west portions of feature C is clearly marked. There is more structure within C, suggestive of more geological variation than in A. The edges of these two features are indicated by high differential curvature. Feature B is enhanced in the differential curvature, consistent with its elongated nature.

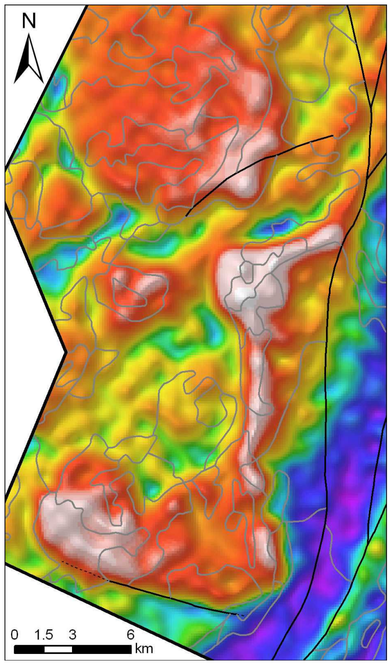

Figure 7. Mean curvature imagery overlain by the published 1:1M geology line work in the Halls Creek Orogen, Western Australia (modified from Stewart, A.J. et al., 2008). Faults are shown with black lines, and geological boundaries are shown with grey lines. Values range from 2.6 x 10^{-9} m^{-1} (red) to -2.6 x 10^{-9} m^{-1} (purple).

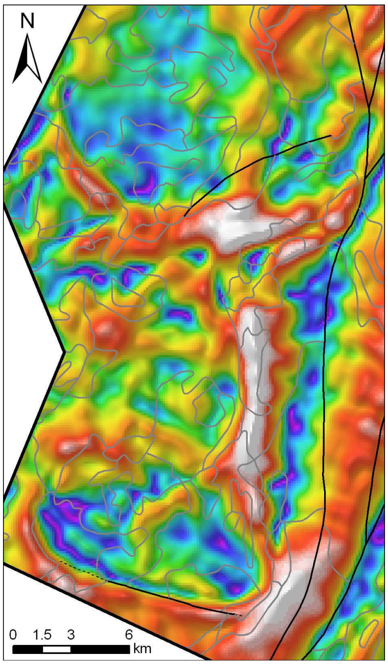

Figure 8. Differential Curvature imagery overlain by the published 1:1M geology line work in the Halls Creek Orogen, Western Australia (modified from Stewart, A.J. et al., 2008). Faults are shown with black lines, and geological boundaries are shown with grey lines. Values range from 4.9 x 10^{-9} m^{-1} (red) to 0.03 x 10^{-9} m^{-1} (purple).

The direction of the minimum curvature follows elongated density structures; conversely, the direction of maximum curvature points towards the largest changes in density sources.

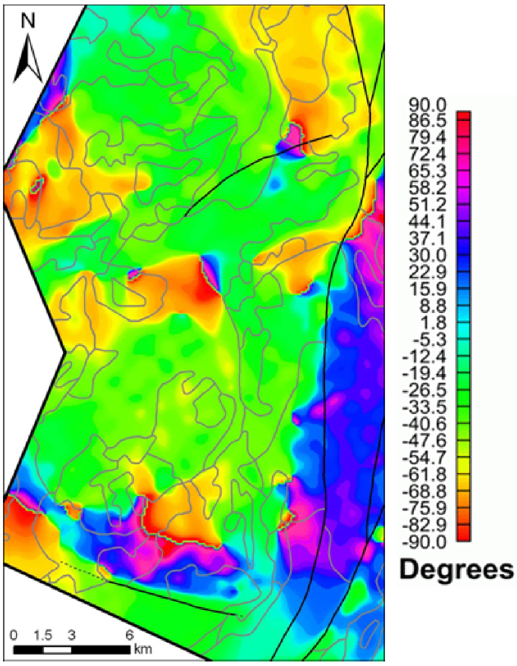

Figure 9. Strike of the Maximum Curvature imagery overlain by the published 1:1M geology line work in the Halls Creek Orogen, Western Australia (modified from Stewart, A.J. et al., 2008). Faults are shown with black lines, and geological boundaries are shown with grey lines. Here, the north-south strikes of maximum curvature (strike angle of 0°) are shown in light blue, while east-west strike angles (either –90° or 90°) appear red.

Curvatures when applied together with other derivative products that include the vertical gravity (gD) and vertical gravity gradient (GDD) improve edge detection and the identification of dipping contacts and/or bodies at depth.

DISCUSSION

Curvatures of the equipotential surface provide us with direct, and readily visualized, information on the physics of the gravity gradiometry tensor. For example, curvature inverses have been shown to yield characteristic distances. Hinojosa and Mickus (2001) suggested that the gravity/gradient ratio (g/φ_{zz}) represents a length scale, and provides a first-order estimate of the depth-to-source of the gravity anomaly. This independent estimate of depth is neither a function of the isostatic model nor of the density contrast producing the gravity anomaly. The maximum and minimum curvatures presented here should provide bounds for this depth estimate.

The modeling and application of curvatures to AGG data has identified that the differential curvature has higher spatial frequency content than the mean curvature, which helps to explain why it has a higher resolving power than other gradients when used in inversions (Condi, 1999).

Because curvatures are an inherent property of the field, they are not dependent on choice of coordinates and are rotationally invariant.

Finally, it can be speculated that all ratios of the form φ_{ij}/g are curvatures. Future work will determine if this is true and useful.

CONCLUSIONS

The gravity gradient tensor has a clear and readily visualised meaning as the curvature of the gravitational potential field, expressed via the curvatures of the equipotential surface and it's normal. The mean curvature can be large only when there is a large nearby mass and so maps of the mean curvature map the variations in mass distribution. The differential curvature, as measured by the FALCON™ airborne gravity gradiometer system, is largest when the curvature is directional and so it maps the edges of bodies and enhances the response from elongated sources. The direction of maximum curvature of the equipotential surface, also derived directly from FALCON™ AGG measurements, maps predominant strike directions in the geology.

The curvature directly ties the measured field to information of interest (location of mass, edges and strike) and it does it in a natural physical way that is easy to understand and visualise. The use of curvatures should improve the understanding, and the geological interpretations, of gravity gradient data.

We have shown that the horizontal gradients of the vertical component of the gravity vector form the curvature of the gravity field line. As this line is orthogonal to the equipotential surface, its curvature is related to how successive equipotential surfaces change and, for surveys covering an extended area, it is redundant.

In principle, the curvatures of the equipotential surface (the differential curvature, the mean curvature and the direction of maximum curvature) contain complete information about the field so that AGG data may be interpreted using only these curvatures.

The curvature method was tested on a synthetic model and applied to FALCON™ AGG data from the Halls Creek Orogen, Western Australia.

ACKNOWLEDGEMENTS

We would like to thank Fugro Airborne Surveys Pty Ltd, Perth, Australia for granting permission to show these data.

REFERENCES

Bell, R. E., and Hansen, R. O., 1998, The rise and fall of early oil field technology: The torsion balance gradiometer: The Leading Edge 17, 81–83.

Condi, F.J., 1999. Estimating Subsurface Structure through Gravity and Gravity Gradiometry Inversion: PhD Thesis.

Heiland, C. A., 1968, Geophysical Exploration, Hafner Publishing Co., New York.

Hinojosa, J.H., and K.L. Mickus, 2001, The Gravity/Gradient Ratio: A First-Order Depth-to-Source Estimate, Eos Transactions, Amer. Geophys. Union, Spring Meeting Suppl., 82 no. 20.

Hofmann-Wellenhof B., and Moritz H., 2006. Physical Geodesy 2nd corrected: Edition Springer-Verlag Wien. 48–52.
Lee, J. B., 2001, FALCON gravity gradiometer technology: Exploration Geophysics 32, 247–250.

Lee, J.B., 2001, Falcon gravity gradiometer technology: Exploration Geophysics, 32, 247-250.

Metzger, E. H., 1977, Recent gravity gradiometer developments: Presented at Guidance and Control Specialist Conference, American Institute of Astronauts and Aeronautics.

——— 1982, Development experience of gravity gradiometer system: IEEE Plans, 323–332.

Pawlowski, B., 1998, Gravity gradiometry in resource exploration: The Leading Edge 17, 51–52

Pedersen, L.B. and T.M. Rasmussen, 1990, The gradient tensor of potential field anomalies: some implications on data collection and data processing of maps: Geophysics, 55, 1558-1566.

Shaw, H., and Lancaster-Jones, E., 1923, Eötvös torsion balance: Proceedings of the Physical Society of London.

——— 1927, The theory and practical use of the Eötvös torsion balance: Mining Magazine 35, 151–166.

Slotnick, M. M., 1932, Curvature of equipotential surface: AAPG Bulletin 16, 1250–1259.

van Leeuwen, E. H., 2000, BHP develops airborne gravity gradiometer for mineral exploration: The Leading Edge 19, 1296–1297.

Sheppard, S. et al. 1997, Compilation of whole-rock analyses from the Halls Creek and King Leopold Orogens, Geological Survey of Western Australia.

Stewart, A.J. et al. 2008, Surface geology of Australia 1:1,000,000 scale, Western Australia [Digital Dataset], Canberra: The Commonwealth of Australia, Geoscience Australia.